

Activity Analysis in Microtubule Videos by Mixture of Hidden Markov Models

Alphan Altinok¹ Motaz El-Saban² Austin J. Peck³ Leslie Wilson³
Stuart C. Feinstein³ B. S. Manjunath² Kenneth Rose²

Computer Science¹, Electrical and Computer Engineering², Molecular, Cellular, and Developmental Biology³
University of California Santa Barbara, Santa Barbara, CA, 93106

alphan@cs.ucsb.edu

Abstract

We present an automated method for the tracking and dynamics modeling of microtubules -a major component of the cytoskeleton- which provides researchers with a previously unattainable level of data analysis and quantification capabilities. The proposed method improves upon the manual tracking and analysis techniques by i) increasing accuracy and quantified sample size in data collection, ii) eliminating user bias and standardizing analysis, iii) making available new features that are impractical to capture manually, iv) enabling statistical extraction of dynamics patterns from cellular processes, and v) greatly reducing required time for entire studies. An automated procedure is proposed to track each resolvable microtubule, whose aggregate activity is then modeled by mixtures of Hidden Markov Models to uncover dynamics patterns of underlying cellular and experimental conditions. Our results support manually established findings on an actual microtubule dataset and illustrate how automated analysis of spatial and temporal patterns offers previously unattainable insights to cellular processes.

1. Introduction

Advances in computer vision and pattern analysis find excellent applications in biological data, specifically in the analysis of patterns on massive image and video libraries. Over the years, researchers generated large amounts of image and video libraries that stimulated research efforts for pattern analysis applications. In this context, microtubule (MT) dynamics research is one of these fields where automated and advanced analysis techniques are anticipated to make a significant and imminent contribution.

MTs are filamentous subcellular structures involved in essential cellular functions. Research on MT dynamics seeks to understand and quantify underlying cellular mechanisms relating to normal and abnormal functioning of the cell in response to changes in environmental conditions [8]. A striking example is as follows: MTs regulate cell divi-

sion by attaching to chromosomes and segregating them in dividing cells, and common conjecture is that certain vital diseases such as Alzheimer's and cancer are at least correlated with the regulatory abnormalities in MT dynamics. A clear understanding of MT activity (behavior) and causal factors may advance the state of the art in medicine.

The main objective in analyzing MT dynamics is quantifying effects of MT associated proteins (MAP) and MT targeting drugs (MTD) on MT behavior. To that end, current methods rely on manual tracking and studies are typically limited by a small number of MTs per experimental condition, such as the presence of a MTD. There are no attempts of analyzing dynamics patterns using computational methods. Potential computational contributions are automating the tracking task and offering pattern analysis techniques. Further details are provided in section 1.1.

We present an automated activity analysis system for MT dynamics, which provides researchers with previously inaccessible data analysis and quantification capabilities. In overview, the procedure consists of computing dynamics features, growth and shortening events, by automatically tracking MTs and extracting activity patterns by mixtures of Hidden Markov Models (HMMs) for indications of potential cellular or experimental regulatory mechanisms, Fig.1. Our results support manually established findings, and illustrate how extraction of temporal patterns offers previously unattainable insights, potentially elucidating novel biological discussion.

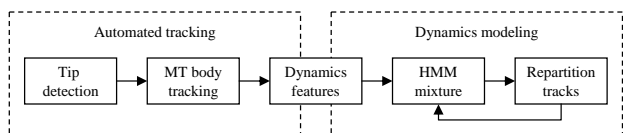


Figure 1. Overview of the proposed system.

Key contributions are i) increasing accuracy and number of tracks collected, ii) eliminating operator bias, iii) computation of new features that are impractical to capture manually, iv) providing analysis tools for MT activity enabling discovery of temporal patterns in cellular processes,

v) standardization of tracking and analysis across MT research labs, and *vi)* reducing required time and effort for entire studies to a fraction.

Next, we present the biological motivation for the proposed system. In section 2, we review previous work in applicable methods. Then we introduce the tracking procedure in section 3. In section 4, we discuss how MT activity is modeled using data from tracking. Following the experiments in section 5, we conclude with a discussion of results in section 6.

1.1. Impact on microtubule dynamics research

MT dynamics research is vital in understanding critical mechanisms in cellular function. Cell division, movement, distribution of nutrients and similar functions are facilitated, in part, by MTs. Main tool of MT dynamics research is to analyze time lapse images of MTs and manually track and quantify observed events, such as growth and shortening, Fig.2, followed by analyzing statistics of events in response to variations of regulatory elements, such as MAPs and MTDs.

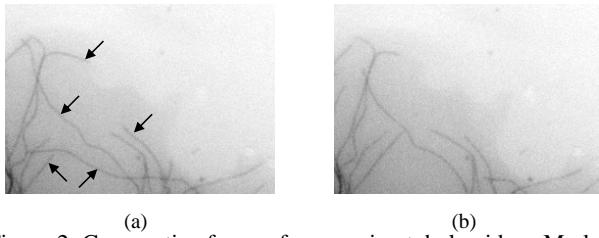


Figure 2. Consecutive frames from a microtubule video. Marked microtubules in (a) are dynamic.

Manual analysis has the following shortcomings: *i)* accuracy (arbitrarily selected reference point, from which Euclidean tip distances in consecutive frames are calculated), *ii)* limited usable sample size (3-5 MTs tracked per video), *iii)* subjectivity (tracking dynamic MTs as they seem more visible), *iv)* variability (research labs differ in data collection and analysis procedures), *v)* limited with traditional dynamics events in a context free manner (each track is parsed into events and treated independent of each other for finding average parameter values like growth rates), and *vi)* span months to years to complete.

Automated tracking provides not only considerably more data per image stack, but also facilitates the computation of other features, such as curving, which cannot be feasibly collected manually. Computational modeling technique, introduced in this paper, keeps contextual information of growth and shortening events intact. By considering an entire *life history* (track) as a unit of MT dynamics (as opposed to frequencies of independent events), researcher are able to establish and examine groups of MTs that exhibit similar dynamic behavior.

Regulatory mechanisms of the cell control the dynamics of MT behavior. However, much of the details of these mechanisms and the functional principles are still unknown. Because we can now estimate models with considerably more dynamics data, we can address questions of commonalities between regulatory mechanisms influencing MT behavior. With the availability of machine learning methods, it will be possible to design biological experiments around the capabilities the offered method. For example, if a cellular switch was hypothesized to alternate the cell's state for regulating MT dynamics, we should expect to observe the switch in action from pre-treatment to post-treatment behaviors of the MTs.

2. Related work

2.1. Microtubule tracking and modeling

In the literature few papers [5, 7, 13, 12, 9, 3] have addressed the MT detection and tracking problems. In [5], the central axis of MTs is estimated by the shortest path on a graph with manually selected end points. In [12], the authors utilize MT shape information to segment MTs using active shape models and Kalman filters. In [9], MTs are extracted in terms of consecutive segments by solving Hamilton-Jacobi equations. The algorithm extracts the MT starting from a manually selected tip. In [7], starting from an initial point on the MT, the MT body is extracted and tracked over frames using tangent constraints. Though the tracking algorithm is automated, the authors report difficulties in handling MT intersections. The main issue with their approach is that MT tracking is carried out using a local measure of consistency that can lead to problems at intersections. To solve this issue, we propose a global multi-frame approach to resolve tracking conflicts. It is worth noting the work done on speckle microscopy [20] where different points are tagged along molecular structures. These tags can be tracked using particle methods. However, for the case of MTs there is no guarantee that the MT tip will be tagged and hence tips dynamics cannot be computed.

On the modeling side, there has been prior work aiming at building physical models for MTs in [17]. We could not locate prior work using machine learning tools to model MT dynamics.

2.2. Detecting and tracking curvilinear structures

MTs are a type of curvilinear structures. Other examples include neuron, retinal blood vessels, road, mammographic and fingerprint images. For example [15] addresses the problem of fully automated tracing of neurons from noisy confocal microscopy images. In [19], the authors present automated tracking methods for the analysis of changes in neuron image sequences. In [11], narrowing of retinal blood vessels is automatically estimated using a vessel tracing al-

gorithm. Besides, many techniques have been proposed to detect general curvilinear structures such as scale space approaches, anisotropic Gauss filtering, fusion of two local line detectors followed by a global Markov random field, using differential geometric properties of images and using active contours. For the problem of matching curvilinear structures between sets of images, in the majority of the proposed methods, lines are first detected and then line properties such as orientation, position, width and center lines are used to establish correspondences [18, 2, 14].

In most of these techniques, binarizing line detector response is a preprocessing step before matching images. In case of noisy video sequences such as MTs, binarization can be very challenging. We believe a more robust approach is to use the continuous response to establish correspondences.

3. Automated tracking of microtubules

There are several challenges facing the automated tracking of MTs:

- MTs are tubular structures with highly variable shapes across the cell. An accurate estimation of MT length must consider the nonlinear shape.
- MT length and body trajectory can undergo large changes from frame to frame with high chance of occlusions.
- MT images have low signal-to-noise ratio and exhibit nonuniform illumination spatially and temporally.

To address the above challenges, we model MTs as flexible open curves in the image plane. We assume one of the ends to be fixed, while the other -*the tip*- is free to move. Formally, a single MT is modeled by the open curve $C(s)$ where $s \in [0, 1]$ is the curve parameter. The goal of the MT tracking task is to estimate 1) the position of the tip and 2) the deformation of the curve forming the MT body, in every frame.

3.1. Estimating MT tip positions

In order to reduce the effect of background noise, MT videos are first processed using a line filter. Let the intensity function in a frame be denoted as I , the output after filtering is then:

$$I^f(x, y) = \max_{\theta}(I(x, y) * G''_{\sigma, \theta}(x, y)) \quad (1)$$

where $G''_{\sigma, \theta}(x, y)$ is a second derivative of Gaussian kernel with scale σ and orientation θ at position (x, y) . σ is chosen experimentally based on the MT width. The motivation behind the use of a second derivative of Gaussian filter kernel is that MTs look like black curvilinear structures on a light background in an ideal scenario. An example of finding

the maximum of a second derivative of Gaussian convolved with the image at all pixel locations is shown in Fig 3.

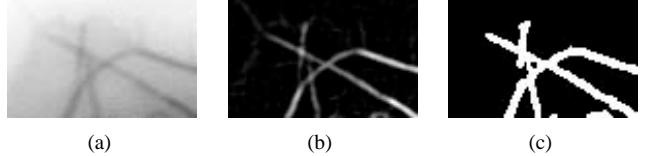


Figure 3. A window, (b) filter output and (c) binarization.

The filtered frames are binarized to generate a mask showing MT polymer mass. The binary mask serves for detecting MT tip candidates in every frame. It is worth noting that though the tip positions are estimated, no correspondence between different frames has been established yet.

We model the problem of matching MT tips between frames to form MT tracks using a graph, constructed globally over the entire video. The main advantages of formulating the matching problem in a spatiotemporal context are

- it can handle missing tips due to noisy conditions by allowing the final MT tracks to skip frames in between,
- it can potentially remove spurious tips found if the noise or signal loss does not occur repeatedly at nearby locations in consecutive frames.

3.1.1 Graph formulation on the video

Consider a MT video of length T frames. Let us denote N_i to be the number of candidate tips detected in frame i for $1 \leq i \leq T$. Then, each detected tip over the entire video can be denoted by t_i^h where i is the frame number, and h corresponds to the tip number within the range $1 \leq h \leq N_i$. We construct a graph $G = (V, E)$ whose vertices V are the detected tips (positions) in every frame and the edges E represent similarity (computed from distance in position) between vertices. The edge weights of the graph represent the matching gain of corresponding two tips in different frames. By allowing edges between vertices in non-consecutive frames, we can generate MT tracks that skip frames in the middle to overcome temporary occlusions.

3.1.2 Edge weights on the graph

Edge weights on the graph G correspond to the similarity measure linking tips in different frames. Consider two tips t_i^h and t_j^r in two different frames f_i and f_j . We can not simply use an inversely proportional measure of the Euclidean distance between tips since this will have problems in cases of tips of different MTs coming in close proximity. A better choice would be to compute a distance between tips constrained on a MT body. The main idea is to test if there is a path along some MT body between the two tips t_i^h and t_j^r . If these two tips come from the same MT, then we have

two cases between frames f_i and f_j : a) the MT is growing and b) the MT is shortening. Since we do not know apriori which case holds, we have to test both.

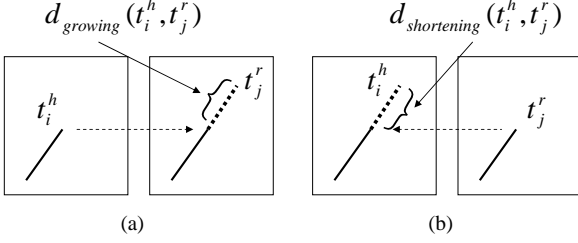


Figure 4. Illustration on how the similarity weight between vertices of the graph is computed between tips in two different frames f_i and f_j . Case of growing (a) and shortening (b).

In the case of a growing MT, we project the location of tip t_i^h on frame f_i to the same location on frame f_j . We compute $d_{growing}(t_i^h, t_j^r)$ as shown on Fig.4(a). In the case of shortening, we project the location of the tip on frame f_j to the same location on frame f_i . The distance $d_{shortening}(t_i^h, t_j^r)$, shown on Fig.4(b) is computed. The similarity metric (edge weight on the graph G) used between the two tips t_i^h and t_j^r is computed as follows:

$$Sim(t_i^h, t_j^r) = e^{-\min(d_{shortening}, d_{growing})} \quad (2)$$

3.1.3 Maximum matching on the graph

Given the graph G of MT tips as vertices and the tip similarities as edge weights, we compute a maximum weight matching of G which corresponds to MT tracks. From graph theory, we know that a *vertex disjoint path cover* C is a covering of G where each vertex of G is in one and only one path of C . The weight of a path cover is defined as the sum of weights on its edges. Using the notion of path cover, the problem of finding the best MT tracks corresponds to finding the *maximum weight path cover* of G with the weights defined by the similarity in (2). Formally, a maximum weight path cover $C(G)$ is a path cover which satisfies:

$$C(G) = \arg \max_{C_i} W(C_i) \quad (3)$$

where $W(C_i) = \sum_{e_{uv} \in C_i} Sim(e_{uv})$ and u, v are two vertices in G for which the similarity is computed as in (2). The maximum weight path cover is computed as suggested in [24].

3.2. MT body estimation

Computing MT length estimates based on tip position only is inaccurate in the case when the MT body is not linear, which is very common in reality. This motivates us to estimate the deformable curve constituting the MT body in

every frame of the MT track. By virtue of the spatiotemporal matching of tips, we now have the tip of a given MT available at each frame. We fix another point on each MT (along the MT body) for all the frames so that we have the two MT ends available at each frame. The technique used to estimate the MT fixed point is detailed in the next subsection. Given the two ends of the MT and an intial curve, we estimate the MT body in each frame using an active contour based on line features. Recall that the MT curve is represented parametrically as $C(s)$ where $s \in [0, 1]$. The internal energy is the usual combination of tension and rigidity of the contour. Being interested in tracking MTs that appear as curvilinear structures in an image $I(x, y)$, we use *ridge* features as the external force $E_{ext}(C(s))$. Ridge features are detected using a second order derivative of a Gaussian $G''_\sigma(x, y)$. Consider the following external force:

$$\nabla E_{ext} = w_1 (-\nabla L) + w_2 L sign(\langle -\nabla L, \vec{N} \rangle) \vec{N} \quad (4)$$

where the first term:

$$-\nabla L(x, y) = -\nabla \frac{1}{1 + |G''_\sigma(x, y) * I(x, y)|^2} \quad (5)$$

is a gradient vector field created from the line detector response $|G''_\sigma(x, y) * I(x, y)|$. The purpose of this vector field is to pull the active contour towards the desired curvilinear structure of the MT. The second term $L sign(\langle -\nabla L, \vec{N} \rangle) \vec{N}$ is a balloon-based term used to help moving the contour in smooth areas (with the sign term inspired by the work of [16]).

Finally, note that in the initial frame of the track (may differ from the initial frame of the video), we find the fixed end of MT by Fast Marching, [23], as detailed in the next section.

3.2.1 Estimating the fixed end position on a MT

The active contour model presented above assumes that the MT fixed end is already available. We proceed as follows to estimate the position of the fixed MT end in the initial frame of the track. Denoting the position of the tip of interest as t_{start} , the goal is to find a point t_{end} on the MT body. First, we define the set P of points satisfying:

$$P = \{(x_i, y_i) \mid \int_{t_{start}}^{t_i} I^f(s) ds < \xi\} \quad (6)$$

where $I^f(\cdot)$ is as defined in (1) and t_i is the parameterization corresponding to the point (x_i, y_i) . Basically, P is the set of points satisfying the condition that the weighted distance from the tip t_{start} is below the threshold th (with

suitable values determined experimentally in the range [0.7–1.5]). We define t_{end} as the point maximizing:

$$t_{end} = \arg \max_{cand \in P} \|t_{start} - t_{cand}\|^2 \quad (7)$$

This is equivalent of finding the closest point to the tip while leading to the least curvature path. The MT body is then traced from t_{start} using a gradient descent procedure. The process of tracing the MT body is shown in Fig. 5.

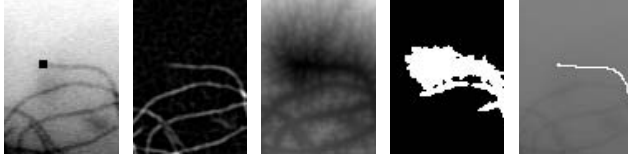


Figure 5. MT body formation: A window around the considered tip in the track with tip overlaid as a black square (a), filtering result used as an input to the distance transform (b), distance transform from the tip with darker values denoting smaller distances (c), points satisfying a distance threshold less than 1 (d), extracted MT body (e).

3.3. Experimental tracking results

We present example tracking results of our proposed technique on real MT video frames. In the spatiotemporal graph matching, we allowed up to three missing frames between tips of the same MT track. The computation of the geodesics is performed using the Fast Marching algorithm. Visual tracking results are shown in Fig. 6. We quantitatively evaluated the tracking performance using manually tracked data as ground truth for 26 MTs in a video sequence. The average duration of MT tracks is 25 frames. The computed mean and standard deviation of error in tracking are 2.85 and 4.36 pixels respectively. This error level is acceptable for biological studies.

Automated tracking delivers on the data collection aspects of the MT dynamics analysis and enables machine learning methods to provide capabilities well beyond the current state-of-the-art. In the next section, we describe our analysis approach.

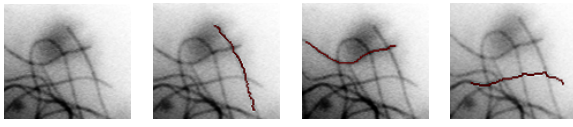


Figure 6. Original microtubules (a), example tracks (b,c,d).

4. Activity modeling

Systematically, MT dynamics statistics under different experimental conditions are analyzed to understand cellular mechanisms, see section 1.1. A limitation in this process is

that statistics consist of mainly average growth and shortening events without contextual information. For example, if growth and shortening events are denoted by g and s , respectively, there is no distinction between tracks consisting of $ggggssss$ and $gsgsgsgs$, despite potential biological significance. Therefore, descriptive activity models can provide invaluable information. Furthermore, such models can be used to ascertain a notion of *distance* between experimental conditions.

Similar dynamics characteristics are known to be shared between different conditions. Conversely, MTs within a cell exhibit dissimilar dynamic behavior patterns. For example, part of the MTs may be transporting molecules within the cell while others may provide motion to the cell. Thus, modeling design should handle expected variations of dynamics within each experimental condition, and similarities between experimental conditions.

Formally, we denote each experimental condition by EC , consisting of groups of dynamic categories w . All experimental conditions have a known label, while patterns making up a condition are unknown, Fig. 7. The problem is to estimate a model λ_i for each category w_i , such that differences between EC_i and EC_j , $i \neq j$, are emphasized.

Note that our formulation calls for a discriminative approach between EC_i , while descriptive models of w_j is the goal within each EC_i .

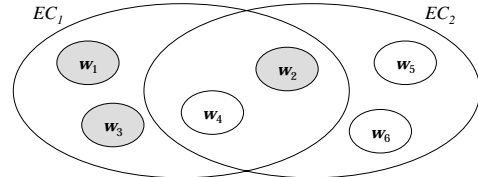


Figure 7. Graphical depiction of experimental conditions EC and dynamics categories w .

A well known class of models used in representing activity is the Hidden Markov Models (HMMs). In the past, they have been used successfully in numerous applications. Particularly in activity context, HMMs were used in human activity recognition [10], abnormal activity detection, gesture recognition, and American sign language recognition. In the next section we present the essential overview of HMMs, while referring the reader to [21] for further details on modeling with HMMs.

4.1. Hidden Markov models

HMMs are probabilistic generative models estimating statistics of a process from observation sequences generated by that process. The modeled process is assumed to be not directly observable, thus *hidden* states capture statistics of the process, subject to stochastic constraints. In practice, hidden states generally correspond to certain physical char-

acteristics of the process. An extensively studied example is sounds in the context of speech recognition [21].

Concisely, HMMs, denoted by λ , are described by parameters $\lambda = (\pi, \mathbf{A}, \mathbf{B})$, where π_i are prior, $a_{ij} \in \mathbf{A}$ are transition, and $b_{ij} \in \mathbf{B}$ are emission probability distributions. Given an observation sequence $\mathbf{O} = (o_1, o_2, \dots, o_T)$, where $t = 1..T$ denotes time, and a model $\lambda = (\pi, \mathbf{A}, \mathbf{B})$, the quantity $P(\mathbf{O}|\lambda)$ can be computed efficiently. Given a set of observation sequences, estimating the parameters of λ is generally performed using maximum likelihood methods, while discriminative techniques were suggested in classification tasks [22, 1].

4.2. Modeling MT dynamics by HMMs

From the biological perspective, classification of tracks to EC is not the end goal for dynamics analysis as EC labels are known a priori. However, estimating λ with descriptive parameters is a significant task. Our formulation of the problem aims to extract patterns through estimating λ , and in doing so we employ the classification score as our measure of model fitness. The problem description motivates us to use a model based clustering approach to estimate λ_i for each w_i . HMM based clustering methods are discussed in [6].

After parameter estimation, each EC is represented by a mixture of λ_i where dynamics variations within an EC are modeled by the components of the mixture. In this sense, λ_i represent the (pseudo)-centers of w_i , where estimating λ_i is primarily a modeling task and cluster forming provides the discrimination between EC .

4.3. Model estimation

We define the quantity $P(\mathbf{O}|\lambda)$ as the similarity measure between the observation sequence \mathbf{O} and the cluster center λ_w of dynamics category w . Expected overall likelihood

$$L = \sum_w \sum_{o \in C_w} \log P(\mathbf{O}|\lambda_w) \quad (8)$$

is maximized by iterating through

- Repartition
 - assign o to cluster C_w such that
 $w = \arg \max_w \log p(o|\lambda_w)$
- Reestimate models
 - train λ_w on C_w , $w = 1..W$

4.4. Evaluation

As mentioned, we utilize the classification accuracy between EC as our measure for overall model reliability. We compute the probability $p(o|EC)$ by

$$p(o|EC) = \sum_{w=1}^W p(o|\lambda_{w,EC}) P_w \quad (9)$$

where P_w is the relative number of cluster members, and estimate the separation by counting correct classifications of tracks $o \in \mathbf{O}$ with

$$EC^* = \arg \max_i [P(o|EC_i)] \quad (10)$$

5. Experiments

In this work, we used the dataset from [4]. 111 videos were collected, each one with 25 frames recorded every 4 seconds.

Growth and shortening rates were computed as the length difference of a MT between consecutive frames, measured in pixels. Thus, each track consists of an observation sequence 25 points in time. Resulting observation sequences were in the range $[-13.03, 11.22]$, where $(-)$ corresponds to shortening and $(+)$ corresponds to growth rates.

Experimentation with both left-right and fully connected HMMs revealed that fully connected models were better suited for the modeling task, in line with biological input. Growth and shortening rates were assumed to be drawn from (single) Gaussian emissions. Since good initialization values are essential with continuous emission distributions, we derived statistics from observation vectors for initializing emissions. Transition and state priors were initialized randomly, and the number of clusters was determined experimentally, Table 3.

The study in [4] analyzes the potential for Taxol[©] (a cancer therapeutic) resistance of different tubulin isoforms. Five experimental conditions were recorded, β III-tubulin (no Taxol treatment), β III-Taxol, β III-Taxol uninduced (Taxol exists in the cell but is inactive), β I-tubulin (no Taxol treatment), and β I-Taxol denoted by EC_1 through EC_5 , respectively. A total of 3068 MTs were tracked from these conditions, with $\{897, 614, 414, 370, 773\}$ tracks in respective EC_i . Results in [4] show that two groups of EC exhibit different dynamics: $\{EC_1, EC_2, EC_4\}$ vs. $\{EC_3, EC_5\}$, where the first group shows suppressed dynamics in terms of the growth and shortening events, as opposed to the latter group. It is also known that EC_4 and EC_5 exhibit different dynamics, where EC_5 is less dynamic than EC_4 .

5.1. Results

The first experiment was designed to confirm biological results. A classification score between EC_4 and EC_5 (denoted by EX:A), and between $\{EC_1, EC_2, EC_4\}$ and $\{EC_3, EC_5\}$ (denoted by EX:B) were computed with a 3-way cross-validation, Table 1. Well defined separations between the two groups and between Taxol-treated and control

	EX:A	EX:B	EX:C
Correct (%)	95.91	94.27	62.67

Table 1. Correct classification rates for EX:A,B,C.

		q_1	q_2	q_3	q_4
λ_1	μ	0.58	0.32	0.56	0.22
	σ	0.61	3.32	0.65	8.32
λ_2	μ	4.03	-2.42	0.48	0.01
	σ	2.17	2.59	0.91	8.08

Table 2. Example emission distributions of λ_1 from EC_4 (Taxol), and λ_2 from EC_5 (non-Taxol), for states q_{1-4} .

W	1	2	3	4	5
Correct (%)	62.11	76.28	94.27	72.33	57.44

Table 3. Change in classification by number of models W .

tracks agree with established biological findings. A third test, denoted by EX:C, was aimed to separate EC_3 from EC_5 . Biological results indicate that these experimental conditions exhibit highly similar dynamics. A maximum separation of much less than EX:A and EX:B verify this finding.

Since the statistics captured in the model parameters are more significant for biological studies than the classification scores, we examined the models of each EC .

Table 2 shows example emission distributions for estimated models from EX:A. Nearly all states of λ_4 show stable distributions, while states in λ_5 show higher dynamic behavior with occasional stable states. Parameters confirm the biological conclusion that Taxol[®]-treated MTs exhibit suppressed dynamics.

Finally, the number of clusters in each EC was determined experimentally, Table 3. Correct classification rates peak at $W = 3$ for EX:B.

Next, we discuss what new analysis capabilities can be provided to researchers by the proposed method.

5.2. Future analysis capabilities

Fig.8 shows a frame of a video from EC_5 , with overlaid tracking results. All tracks are evaluated for $p(o|EC_4)$, and $p(o|EC_5)$. $p(o|EC_5)$ values are shown for selected tracks for illustration purposes. The upper left track is an erroneous track of an image artifact, while others are actual MT tracks. By evaluating each track with estimated models and overlaying the results on the frame, it is possible to visualize the dynamics relationship of all tracked MTs with respect to known models.

Furthermore, distance measures between models or

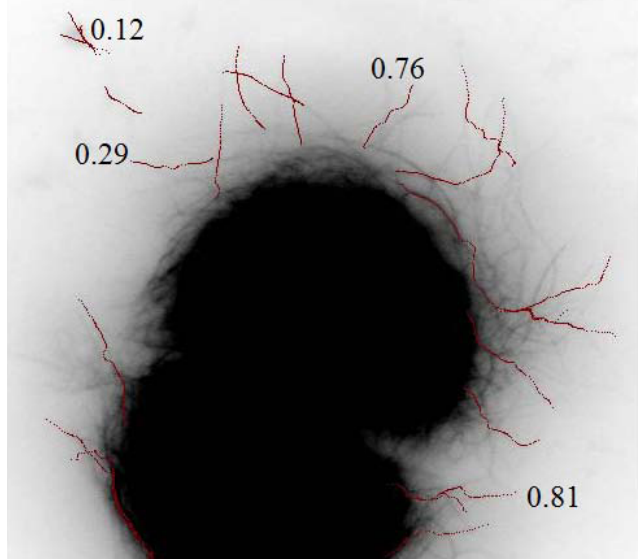


Figure 8. Tracked MTs with associated $p(o|EC_5)$.

model mixtures can be defined to quantify aggregate dissimilarities between dynamics pattern. An example distance measure between models can be found in [21].

Finally, models can be estimated not only for traditional dynamics parameters, but for any combination of biologically significant data. An example feature set that is readily available by the tracking component of the proposed system is the degree of curviness as a function of time. Such features offer significant information, yet they are nearly impossible to collect manually.

5.3. Discussion

Our modeling approach considers individual MTs from various conditions as the basis of observations and does not make a distinction between cells from which MTs were tracked. An alternative analysis can be performed by treating each cell as the observation vector and models can be estimated for activity of various cell lines.

Note that tracking may generate occasional erroneous tracks by following image artifacts, losing a track prematurely, and so on. Estimated models provide an added layer of robustness by encoding relevant patterns of dynamics from computed tracks. Furthermore, noise may be explicitly modeled by dedicating a component of the model mixture for this purpose. For example, Table 2 shows large deviations in the last states of each model. Further investigation may reveal the cause and meaning of such deviations, possibly as noise.

6. Conclusion

In this work, we presented an activity analysis system for MT dynamics research. Most notable contribution of the

proposed method is the novel analysis capabilities that are beyond the current state-of-the-art. Other contributions are the radical improvements over the manual data collection methods, such as higher accuracy (length along MT body vs Euclidean estimate), larger samples (3068 automated vs 339 manual) and objective consideration of all MT tracks at a fraction of the normally required time. Our results support manually established findings, and show that automated analysis of spatial and temporal patterns offers previously unattainable insights. Most notably, the standardization of data collection and analysis facilitates a comparative platform for future biological research.

As the volume and number of dynamics datasets has increased in recent years, similarities between the behavioral influence of MAPs and MTDs upon dynamics have emerged, leading to speculation of similar mechanisms. Dynamics models may facilitate the union of previously isolated MAP and MTD datasets, furthering our understanding of regulatory mechanisms of MTs.

Despite the difficulty in assessing performance of the method, we hope that our work will serve as the ground truth for future advances in this direction.

7. Acknowledgements

This study was funded by the Center for Bioimage Informatics under grant NSF-ITR 0331697.

References

- [1] L. R. e. a. Bahl. Maximum mutual information estimation of hidden markov model parameters. *Proc. Int. Conf. Acoustic, Speech, Signal Processing*, 1:4952, 1986. [6](#)
- [2] Y.-L. Chang and J. Aggarwal. Line correspondences from cooperating spatial and temporal grouping processes for a sequence of images. *Computer Vision and Image Understanding*, 67(2):186–201, Aug 1997. [3](#)
- [3] G. Danuser, P. Tran, and E. Salmon. Tracking differential interference contrast diffraction line images with nanometre sensitivity. *Journal of Microscopy*, 198, pages 34–53. [2](#)
- [4] K. K. et al. β iii-tubulin induces paclitaxel resistance in association with reduced effects on microtubule dynamic instability. *J. Biol. Chem.*, 280(13):12902–12907, Apr 2005. [6](#)
- [5] L. L. et al. Extraction of 3d microtubules axes from cellular electron tomography images. In *Proc. of ICPR*, volume 1, pages 804–807, 2002. [2](#)
- [6] M. B. et al. *Similarity-Based Clustering of Sequences Using Hidden Markov Models*, volume 2734. Springer-Verlag GmbH, 2003. [6](#)
- [7] S. H. et al. Automatic quantification of microtubule dynamics. In *Proc. of Int. Symp. on Biomedical Imaging: From Nano to Macro*, 2004. [2](#)
- [8] S. C. Feinstein and L. Wilson. Inability of tau to properly regulate neuronal microtubule dynamics: a loss-of-function mechanism by which tau might mediate neuronal cell death. *Biochim Biophys Acta*, page 268279, 2005. [1](#)
- [9] S. Hadjidemetriou, D. Toomre, and J. S. Duncan. Segmentation and 3d reconstruction of microtubules in total internal reflection fluorescence microscopy (tirfm). In *8th International Conference on Medical Image Computing and Computer Assisted Intervention, (MICCAI)*, 2005. [2](#)
- [10] S. Hongeng, B. F., and N. R. Representation and optimal recognition of human activities. In *CVPR*, volume 1, pages 818–825, 2000. [5](#)
- [11] W. M. L. L. T. Y. W. Huiqi Li; Hsu. Automatic grading of retinal vessel caliber. In *IEEE Transactions on Biomedical Engineering*, volume 52, pages 1352 – 1355, 7 2005. [2](#)
- [12] M. Jiang, Q. Ji, and B. F. McEwen. Model-based automated segmentation of kinetochore microtubule from electron tomography. In *Proc. of 26th Annual International Conference of the Engineering in Medicine and Biology Society*, 2004. [2](#)
- [13] M. Jiang, Q. Ji, and B. F. McEwen. Automated extraction of microtubules and their plus-ends. In *WACV/MOTION 2005*, pages 336–341, 2005. [2](#)
- [14] B. Kamgar-Parsi. Algorithms for matching 3d line sets. *IEEE Transactions on Pattern Analysis and Machine Intelligence*, 26(5):582–593, May 2004. [3](#)
- [15] M. I. S. L. D. H. S. N. D.-M. W. S. J. N. T. Khalid A. Al-Kofahi, Ali Can and I. Badrinath Roysam, Member. Median-based robust algorithms for tracing neurons from noisy confocal microscope images. In *IEEE Transactions on information technology in biomedicine*, volume 7, 2003. [2](#)
- [16] R. Kimmel and A. Bruckstein. Regularized laplacian zero crossings as optimal edge integrators. *International Journal of Computer Vision*, 53(3):225–243, 2003. [4](#)
- [17] e. a. Maddox P. Direct observation of microtubule dynamics at kinetochores in xenopus extract spindles. *Journal of Cell Biology*, 162:377–382, 2003. [2](#)
- [18] R. Marti, R. Zwiggelaar, and C. Rubin. Tracking mammographic structures over time. In *British machine vision conference*, 2001. [3](#)
- [19] A.-K. Omar and R. Richard. Automated semantic analysis of changes in image sequences of neurons in culture. In *IEEE Transactions on Biomedical Engineering: Accepted for future publication*, volume PP, pages 1–1, 2006. [2](#)
- [20] V. P., E. Salmon, W.-S. C., and D. G. Recovery, visualization, and analysis of actin and tubulin polymer flow in live cells: A fluorescent speckle microscopy study. *Biophys. J.*, 85:1289–1306. [2](#)
- [21] L. Rabiner and B. H. Juang. *Fundamentals of Speech Recognition*. Prentice-Hall, 1993. [5](#), [6](#), [7](#)
- [22] A. Rao and K. Rose. Deterministically annealed design of hidden marov model speech recognizers. *IEEE Trans. On Speech and Audio Processing*, 2001. [6](#)
- [23] J. Sethian. *Level Set Methods and Fast Marching Methods*. Cambridge Univ. Press, 1999. [4](#)
- [24] K. Shafique and M. Shah. A noniterative greedy algorithm for multiframe point correspondence. *IEEE Transactions on Pattern Analysis and Machine Intelligence*, 27(1):51–65, Jan 2005. [4](#)